Renewable Energy 149 (2020) 735–748

Contents lists available at ScienceDirect

Renewable Energy

journal homepage: www.elsevier.com/locate/renene

The near-field of a lab-scale wind turbine in tailored turbulent shear flows

L. Li [a, *], R.J. Hearst [a], M.A. Ferreira [b], B. Ganapathisubramani [b]

[a] Department of Energy and Process Engineering, Norwegian University of Science and Technology, Trondheim, Norway
[b] Engineering and Physical Sciences, University of Southampton, Southampton, UK

ARTICLE INFO

Article history:
Received 16 April 2019
Received in revised form
21 November 2019
Accepted 9 December 2019
Available online 13 December 2019

Keywords:
Wind turbine
Tailored turbulence
Shear flow
Lab-scale

ABSTRACT

Real wind turbines experience a wide range of turbulent shear flows that naturally occur within the atmospheric boundary layer, however, these are often difficult to simulate in experiments. An active grid was used to expand the testable parameter space compared to conventional methods. Specific focus was placed on decoupling the shear from the turbulence intensity. Particle image velocimetry was used to capture the mean velocity and velocity fluctuation fields in the near-field wake of a model wind turbine subjected to seven different combinations of shear and turbulence intensity. It was found that if the incoming mean profile was removed, the velocity deficit is approximately symmetric about the hub, even for highly sheared cases. The absolute wake velocity deficit profiles are asymmetric for the sheared cases, and the combination of the wake and shear flow results in a local increase in shear on the high-velocity side of the wake immediately downstream of the turbine. This in turn leads to higher turbulence production within that region, leading to larger velocity fluctuations. It is also demonstrated that the mean power of the model turbine is not particularly sensitive to the incoming shear, but the power fluctuations scale linearly with the incoming turbulence intensity.

1. Introduction

Wind turbines are often grouped together in wind farms. As a result, many individual turbines operate in the wakes of upstream turbines. The velocity deficit caused by one or more combinations of wind turbine wakes can lead to significant reductions in power. For instance, Adaramola & Krogstad [1] found a 20%–46% reduction in power output for individual turbines depending on local environment and wind farm layout. Although power losses can be reduced through careful layout planning, the total power loss is still between 10% and 20% compared to an ideal case where every turbine is in the freestream [2,3]. In addition to velocity deficit, the high degree of velocity fluctuations present in the wake causes periodic aerodynamic loading on the blades of downstream turbines, leading to shorter lifespans and higher maintenance costs [3]. Vermeer et al. [4] published an extensive review of available experimental and numerical studies of wind turbine wake structures, and highlighted the need for systematic investigations into the wake structures behind individual wind turbine and wind farms, especially in the near-field wake region.

Adding to the complexity of wind turbine wakes is the fact that wind turbines operate within the atmospheric boundary layer (ABL) where significant shear and freestream turbulence (FST) exist. Modern wind turbines can have rotor diameters around 120 m, and with a tower height of around 100 m, this means that rotors can cover a height from 40 m to 160 m, spanning a non-negligible portion of the ABL, which has thickness on the order of hundreds of meters [5]. The shear flow profile is often parameterized for wind turbine applications as a power-law of the form,

$$\frac{U(z)}{U_r} = \left(\frac{z}{z_r}\right)^{\alpha}, \tag{1}$$

where z is the vertical direction and $U(z)$ is the freestream velocity profile in the wall-normal direction (as a function of z). The subscript r denotes a reference location where U_r and z_r are measured [6]. For a neutrally buoyant atmospheric boundary layer $\alpha \approx 0.143$, and for uniform flow $\alpha = 0$. In the real-world, however, there are significant variations in shear profiles. Wagner et al. [7] classified 2340 independent atmospheric shear measurements into 173 different profiles, and Wagner et al. [6] found that 396 out of

* Corresponding author.
E-mail addresses: leon.li@ntnu.no (L. Li), jason.hearst@ntnu.no (R.J. Hearst).

https://doi.org/10.1016/j.renene.2019.12.049

907, or 44% of their real-world shear profiles at their measurement station could not be adequately described by Equation (1). Furthermore, Dimitrov et al. [8] showed that α has dependencies on both mean wind speed and turbulence intensity, and can range from −0.20 to 0.36. The turbulence intensity experienced by wind turbines also has a wide range of values due to different surface roughness, upstream terrain obstacles and natural oscillations in the atmospheric winds. The survey by Mücke et al. [9] found that turbulence intensity measured from 50 m to 150 m at GROWIAN was typically between 5% and 15%, with gusts reaching up to more than 40%. The high variance in turbulence can have significant impact on wind turbine operations. Milan et al. [10] found that a wind farm's power output can vary by as much as 50% in a time-span of only 2 min, with extreme power changes up to 15 standard deviations occurring on the order of seconds. Therefore, it is evident that most real turbulent shear flows cannot be adequately described by a single or even a few profiles, and thus there is a need to determine the impact of shear and turbulence intensity on a wind turbine in general.

In order to account for the variation in local velocity across the swept area of a wind turbine, Wagner et al. [7] developed a discretized formulation of an equivalent velocity to replace the hub centreline velocity often used in wind turbine power calculations. The equivalent velocity is of the form

$$U_{\mathrm{eq}} = \left[\frac{1}{A}\left(\sum_i \overline{U_i^3} A_i\right)\right]^{1/3}, \tag{2}$$

where A is the frontal swept area of the wind turbine, and the subscript i denotes discretized segments across the span of the rotor. Both U_i and A_i are functions of z. Choukulkar et al. [11] expanded this expression to include the influence from freestream turbulence intensity and yaw angle, via

$$U_{\mathrm{eq,turb}} = \left\{\frac{1}{A}\sum_i \overline{U_i^3}\left[1+3\left(\frac{u_i'}{\overline{U_i}}\right)^2\right]\left[1-\frac{\overline{\phi_i^2}}{2}-\frac{\phi_i'^2}{2}\right]^3 A_i\right\}^{1/3}, \tag{3}$$

where u'_i is the velocity fluctuation, φ_i is the incoming wind angle, and φ'_i is the wind angle fluctuation. It can be seen that an increase in velocity fluctuation will increase the U_{eq} for the same mean velocity profile.

Several methodologies have been used to generate turbulent shear flows in a laboratory setting. The simplest method is augmenting the naturally developing boundary layer on the walls with a series of spires. Using this technique, Counihan [12,13] was able to reproduce both a neutral atmospheric boundary layer and an urban boundary layer with $\alpha = 0.28$, with average turbulence intensities around 7.5%. A more recent effort by Vanderwel & Tavoularis [14] to generate homogeneous turbulent shear flow used a combination of a shear generator and a flow straightener. The main drawback of these passive techniques is that they can only cover a limited range of the parameter space that describes a realistic turbulence shear flow, and each setup needs to be specifically tailored to meet a single set of parameters. On the effects of freestream turbulence alone, it has been shown that an increased freestream turbulence level reduces wake width due to the increased transport of momentum from the freestream into the wake [15]. However this effect was only observed for regions more than two rotor diameters downstream. The same observation was made by Hattori et al. [16]. Both of these studies used passive grids to generate freestream turbulence; Medici & Alfredsson [15] compared clean flow to one grid turbulence flow at 4.5% FST, while Hattori et al. [16] used 4 different grids to generate FST ranging from 7.5% to 15%. However these studies were also limited in their ability to explore a wider parameter space as a result of their physical setup. In particular, most passive set-ups have focused on reproducing the neutral stability conditions, because this is a reasonably well-understood theoretical state. However, the field measurements of Wagner et al. [7] did not identify this profile as one of the 10 most likely to occur at their site, and therefore it may not actually be particularly representative of the flows encountered by wind turbines. Overall, using passive flow modification devices has been successful in producing a few basic examples of turbulent shear flows, but they are not well suited to expand this parameter space or separate shear from turbulence profiles.

The advent of active grids has opened a new frontier of possibilities in producing a wide range of tailored turbulent flow with a single setup. First popularized by the seminal work of Makita [17], active grids have since been used in a variety of studies. The general operational principle of these devices is that a grid of square wings can be actuated in a controlled sequence to augment the turbulence produced downstream; for example, controlled patterns to recreate time-series of field measurements, or random motions that produce turbulence that is approximately homogeneous in transverse planes and locally isotropic. Recently, several studies have used active grids to generate highly-tailored inflow conditions for wind turbine or ABL experiments. Knebel et al. [18] generated highly intermittent turbulent wind fields through the use of an active grid in a wind tunnel, and Neunaber et al. [19] studied the effects of continuous and intermittent turbulent inflows on wake development behind a wind turbine. Shen & Warhaft [20] were the first to incorporate an active grid in a shear flow study by inserting variable solidity screens downstream of the active grid, and later Cekli & van de Water [21] were the first to attempt to create shear flow with an active grid alone. This was accomplished by setting the initial positions of the wings to different angles, and then having each set of wings flap about this angle. Schottler et al. [22] set their active wings to two sets of static positions to create a classical and an inverted shear profile. Rockel et al. [23] used an active grid in passive and active modes to create inflow conditions with low and high turbulence intensities and found that with increasing turbulence intensity, the vortex shedding from the blade tips are destabilized. Talavera & Shu [24] created three different simulations of turbulent ABLs using a single active grid setup, with turbulence intensities ranging from 3% to 17.4% at the centre of the turbine. However they did not explore the possibility of creating different shear velocity profiles in their study. Hearst & Ganapathisubramani [25] were the first to decouple shear and turbulence intensity. This was accomplished by using one plane of wings to create different porosity, and thus shear flow, and the other plane of wings to produce different turbulence intensity levels. The method for producing shear differs slightly between Cekli & van de Water [21] and Hearst & Ganapathisubramani [25], in that Hearst & Ganapathisubramani [25] initially set all the wings parallel to the flow, and oscillated each set of wings by different amplitudes. The work by Hearst & Ganapathisubramani [25] offered unprecedented freedom to explore a large number of parameters for turbulent shear flows with one single setup, and forms the basis for the present study.

2. Experimental procedure

The present experiments were carried out in the University of Southampton's open loop suction wind tunnel, which has a test section measuring 0.9 m × 0.6 m × 4.5 m. The freestream turbulence intensity is approximately 0.2% in the empty tunnel.

The same active grid used by Hearst & Ganapathisubramani [25] and Dogan et al. [26] was used here. The design of the grid is similar to those found in past studies, such as Makita [17] and Hearst &

Lavoie [27]. The grid consists of 11 × 7 rods in a bi-planar layout. Each rod has a diameter of 10 mm. The mesh length $M = 81$ mm is defined as the spacing between the rods. The rods are controlled independently by a computer via 18 daisy-chained stepper motors. Mounted to the rods are square wings with sides measuring 55.86 mm. Solid square wings were used, resulting in a maximum blockage of 100% when all wings are perpendicular to the flow, however, this is never allowed to happen. The active grid was mounted at the inlet of the test section, just after the contraction.

The model wind turbine, detailed in Fig. 1, was designed to achieve a blockage ratio below 7%, including its swept area and the exposed cross-sectional area of the tower. It was driven at fixed, predetermined velocities by a Kollmorgan AKM33H servo motor that was mounted below the test section, coupled to a Futek FSH01987 torque sensor that is accurate to ±20 mNm. A 5 mm diameter driveshaft runs through the tower and is coupled to the horizontal turbine shaft via a built-in right-angle bevel gearbox. A series of ball-bearings at critical locations prevent wobbling and the transmission of vibrations into the system. The tower was built in the form of a NACA0020 airfoil to minimise wake interference with measurements downstream, and is tapered towards the top to increase the surface area in contact with the base plate, which is in turn bolted onto the wind tunnel floor. The profile of the tower fairing does not represent the tower of a real wind turbine, but rather is meant to be a low-flow-disturbance sting. Thus, the rig approximately represents a 'floating' turbine positioned in the centre of the tunnel.

A three-blade rotor, 208 mm diameter, was designed based on the NACA4418 airfoil with a uniform chord distribution $c = 20$ mm. The blade twist profile comes from the NREL reference airfoil [28]. It is mounted to the test section floor 3.05 m downstream of the active grid, corresponding to $37.7M$. The specified rotational velocity was $\omega = 15$ Hz for all cases. It has previously been demonstrated that the wakes of motor-driven and flow-driven wind turbines at this scale are comparable [29]. As the rotational velocity of the turbine was actively kept constant by the control system, the torque (τ) could be used to measure the power from $P = \omega\tau$. A decrease in the power of the system represents an increase in energy extraction because the power does not need to be supplied by the servomotor. Setting the hub centreline freestream velocity at 10 m/s gave a tip speed ratio (TSR) $\lambda \equiv \omega R/U_0 \approx 1$, where R is the radius of the rotor assembly. This is the highest TSR that could be achieved without mechanical vibrations becoming a problem. While we understand that this imposed a limitation to the present study, it is of similar magnitude to the typical TSR of 2–14 found in real wind turbines [30] and we present this study as a demonstration of the experimental capabilities of this approach to model testing rather than as a direct comparison to a full-scale rotor.

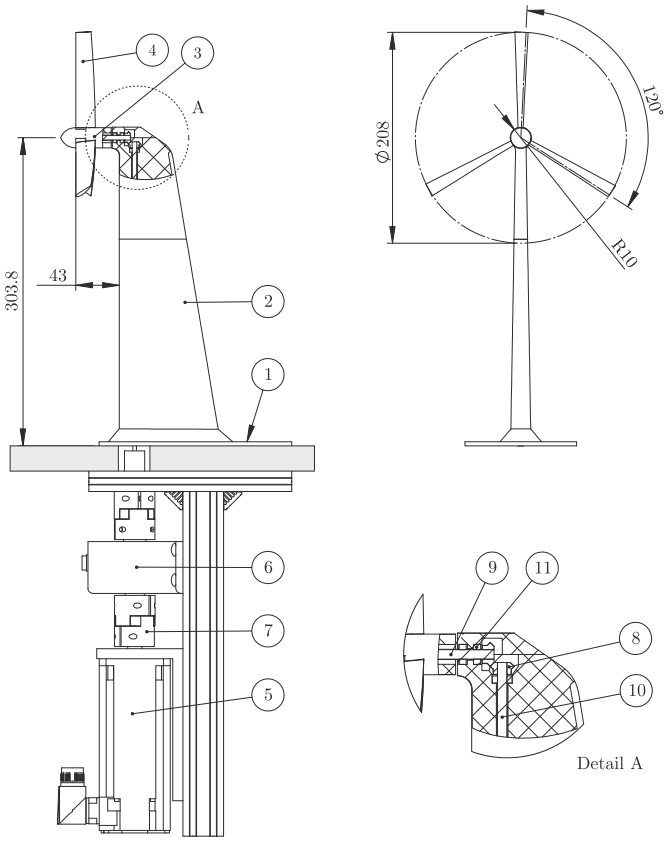

Fig. 1. Model wind turbine design, with side-view on left, front view on the upper-right corner, and a breakout section detailing the bevel gearbox at the bottom right. (1) base plate; (2) tower; (3) hub; (4) blades; (5) motor; (6) torque encoder; (7) coupling; (8) right-angle bevel gearbox; (9) turbine shaft; (10) vertical driveshaft; (11) ball-bearing. Dimensions are in millimetres.

The coordinate system used for this study is identical to the one used by Hearst & Ganapathisubramani [25]; and shown in Fig. 2. The side of the active grid with more degrees-of-freedom was used to create shear flow because it offered greater control for creating different profiles. The z-axis was chosen to coincide with this dimension in order to keep the standard convention of aligning the z-axis with the vertical plane used in atmospheric boundary layer and real wind turbine studies, e.g., Refs. [6,8,9], and [12].

An extended laser sheet upstream and downstream of the wind turbine model was created with two synchronised Litron Nd:YAG lasers (532 nm, 200 mJ per pulse). The laser plane coincides with the hub centreline. Two LaVision ImagerProLX 16 mega-pixel cameras equipped with Sigma DG 50 mm lenses were placed along the streamwise direction. The total field-of-view (FoV) of the two-camera set up was 338 mm wide and 730 mm long. The overlapping region between the FoV from individual cameras is 66 mm long, or about 13% of the length of each camera's FoV. For the laminar uniform flow baseline case, 600 image pairs were acquired, while for all the other test cases 1200 image pairs were acquired. All image pairs were acquired at 0.6 Hz.

Vector fields were calculated with DaVis 8.4.0 on central processing units, beginning with a single pass on a coarse grid of 128 pixels × 128 pixels and then down to three passes at a finer grid of 32 pixels × 32 pixels, with a 50% overlap for each pass. Vector field stitching was done post-calculation in MATLAB using a weighted blend of error and linear functions for averaging and smoothing the overlapping regions between the two frames. Fig. 3 shows representative instantaneous flow fields for all the test cases. While the details of these test cases will be discussed in the next section, we would like to highlight some of the qualitative differences observed in Fig. 3. The reference case REF has the most homogeneous incoming flow and the smallest turbulence intensity. Cases 0L and 0H are uniform flows with higher turbulence intensities, and this can be seen through the increasing prominence of randomly distributed high- and low-velocity regions in the incoming flow. The other cases are shear flows, and have distinctly stratified high- and low-velocity regions in the incoming flow, representing velocities below and above the hub centreline velocity, respectively.

3. Incoming flow conditions

A total of seven different incoming flow conditions were generated for this study. They are the same as those in Hearst & Ganapathisubramani [25], where a more detailed description of the flow conditions can be found. A brief summary will be given here.

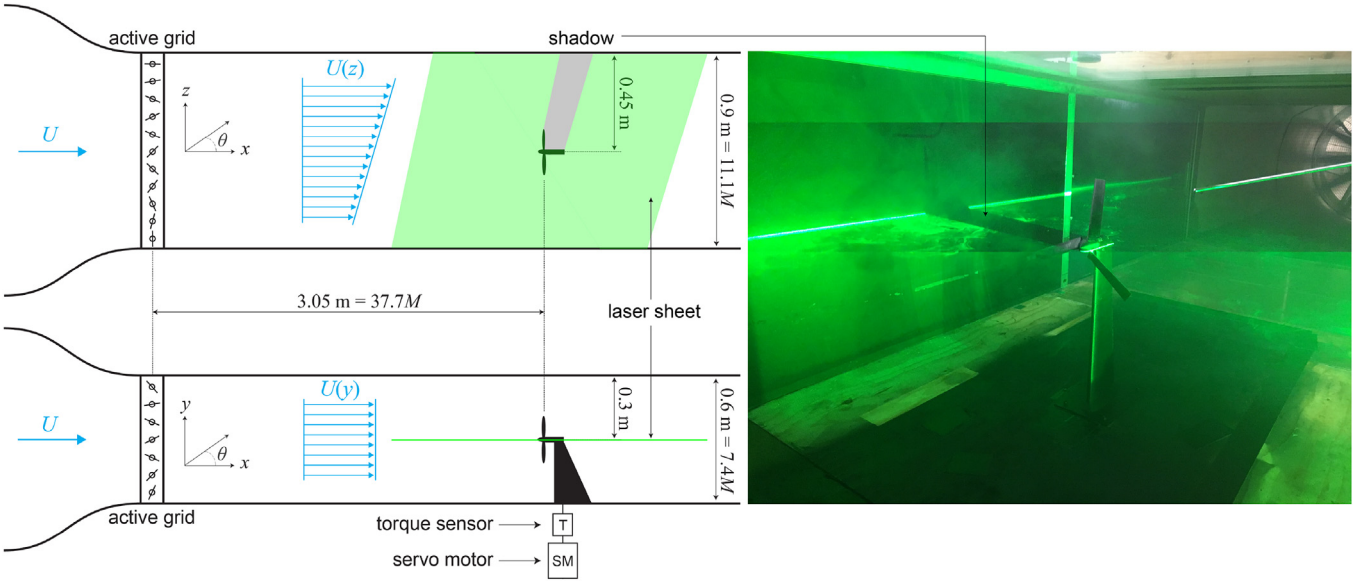

Fig. 2. Schematic of the experimental setup.

Shear was created by oscillating the 11 vertical bars through different angles ranging from 0° to 90°. A small oscillation angle creates a larger apparent porosity, leading to higher local velocity, and vice versa. For this study, three different shear profiles were chosen from the available list in Hearst & Ganapathisubramani [25]. The cases were chosen to represent a variety of turbulence and shear conditions. An additional uniform flow case was added to provide baseline measurements. The shear flow profiles are shown in Fig. 4a, where the incoming flow profile is denoted as U_i. The seven horizontal bars were used to vary the incoming turbulence intensity. The input control parameters were rotational velocity of the wing, rotation duration, and acceleration. The fully random mode of actuation described in Hearst & Lavoie [27] is used here, where each motor is given a sequence of random values of these three control parameters. A measurement was also taken with the active grid removed to obtain a "laminar" flow baseline. The turbulence intensity (u'/U) profiles are shown in Fig. 4b. Fig. 4c and d shows the w-component velocity fluctuation and turbulence isotropy, respectively. The isotropy is comparable to values from other studies that used an active grid to generate freestream turbulence (e.g. Hearst & Lavoie [27]).

A naming convention was developed for the seven incoming flow fields. The baseline case with no grid is denoted as "REF" for reference, and all others were assigned two-character names. The first is a number denoting shear profile shape, and the second is a letter denoting u'/U level. For shear profile shapes, 0 denotes uniform flow, 1 & 2 denote power law profiles with increasing shear gradient (i.e. 2M would have a greater gradient than 1M), and 3 denotes non-power-law profiles. For turbulence intensity the letters L, M, and H are used to denote low, medium and high intensities. Low intensity is defined as less than 5%, medium intensity is defined as between 5% and 13%, and high intensity is defined as 13% or higher.

The freestream mean velocity (U_i) and u'/U profiles shown in Fig. 4 are all computed from the calculated PIV vector fields. The incoming fields are calculated for the range $-0.8 \leq x/D \leq -0.7$. This location corresponds to $35.5M$ downstream from the active grid, which is within the region where grid-generated turbulence is normally considered homogeneous [27,31]. The homogeneity at the turbine location was presented by Hearst & Ganapathisubramani [25] and shown to be strong for a region that exceeds the rotor area. Table 1 lists the α values and turbulence intensities at hub height for all cases. The parameter α is calculated through the same method as described in Hearst & Ganapathisubramani [25]. The minor differences between the incoming flow parameters shown here and in [25] can be attributed to the difference in the PIV of the present measurements compared to the earlier hot-wire measurements.

4. Mean velocity fields

Fig. 5a shows the wake velocity profiles at $x/D = 1$, 1.5, & 2 normalized by the incoming hub centreline velocity U_0. This is a measure of the absolute velocity in the wake region. The incoming profiles at $x/D = -0.7$ are superimposed for comparison with the wake velocity gradient. The absolute wake velocity profiles are symmetric about the hub for the uniform flow cases, as expected. However, for the shear flows, the distributions are skewed by the incoming flow and thus asymmetric. It can also be seen in Fig. 5a that the wake core velocity is approximately the same for all cases. These two effects combine to create a wake velocity gradient that increases with incoming velocity gradient on the high-velocity side, and this wake velocity gradient is greater than that of the incoming flow. While this could imply that subsequent turbines downstream could potentially experience an incoming flow with increased shear, this study is limited to the near-field wake behaviour and further investigations are required to examine wake recovery farther downstream.

It is postulated that this asymmetry in the absolute wake velocity profiles for shear flows is due to the superposition of the incoming shear with the wake. Fig. 5b shows the relative wake velocity profiles at the same downstream locations as in Fig. 5a. These profiles are normalized by having the incoming velocity profiles removed, i.e., $(U - U_i)/U_0$. The relative wake velocity profiles are symmetric about the hub for all test cases, suggesting that the asymmetry found in the absolute wake profiles is indeed caused by the incoming sheared flow. This has significance for modelling the averaged velocity field in the near-wake region, in that the field can be modelled as a linear addition of a wake profile from a uniform flow, and an incoming shear flow, as suggested by

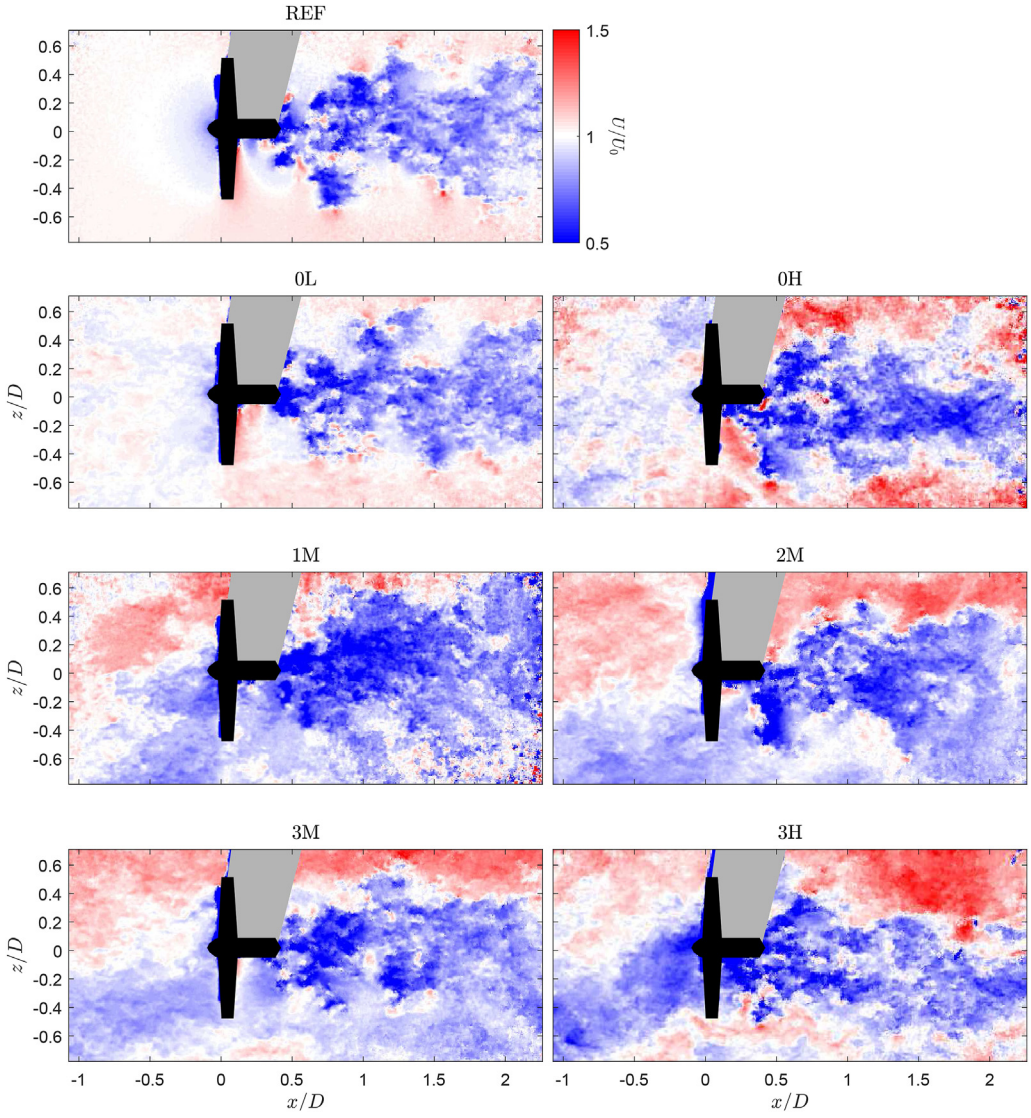

Fig. 3. Representative instantaneous normalized U velocity field for all seven test cases.

Chamorro & Porté-Agel [32]. Fig. 5b also shows reasonable collapse between profiles for a given downstream location, indicating that the macroscopic wake behaviour does not vary significantly with respect to the incoming flow. The two cases with the lowest incoming turbulence intensity, REF and 0L, have wake profiles that are less smooth. It can be seen in Fig. 5b that these two cases have additional relative velocity deficit "bumps" between $0.3 < |z/D| < 0.5$ compared to the other cases. The locations of these bumps corresponds to strong vortex streaks downstream of the rotor tips, which are absent from the higher turbulence intensity cases (Fig. 6). This is expected as higher turbulence intensity promotes mixing in the wake [33], thus producing a wake profile without the additional velocity deficit peaks associated with the rotor tips. The location of the rotor tip vortex streak can be more readily seen in Fig. 7, where the cross-sectional averaged vorticity is shown for $x/D = 1$, 1.5, and 2. The rotor tip vortex streaks for cases REF and 0L are centred at $z/D \sim \pm 0.5$ and are pronounced compared to the other cases. Cases REF and 0L also show a slightly higher velocity deficit at $x/D = 2$ compared with the rest. Again this is expected as higher incoming turbulence level transports more flow from the free-stream into the wake, promoting wake recovery [15]. This is only observed at $x/D = 2$, which is also consistent with the findings of Medici & Alfredsson [15], in that the near-field wake is not significantly affected by different incoming turbulence levels for region $x/D < 2$.

Overall, the absolute and relative wake velocity profiles show that in the presence of a shear flow, the average wake velocity profiles can be linearly decomposed into a symmetric component associated with the wake in a uniform flow, and an asymmetric component that is the incoming shear profile. This is significant because it shows that wind turbine wakes are relatively robust to different incoming turbulent shear flows, and the interactions between the turbine and the different flow conditions produce no observable non-linear effects on the average velocity field in the near-wake. This assertion is more rigorously tested and validated by the present measurements than in previous studies that investigated only a pair of test cases. We would like to note that this observation only applies to the average velocity field, and not the higher-order turbulence statistics.

To further examine the robustness of the near-field relative wake profiles to the different incoming flows, the wake geometries are extracted from the velocity fields for all the test cases and

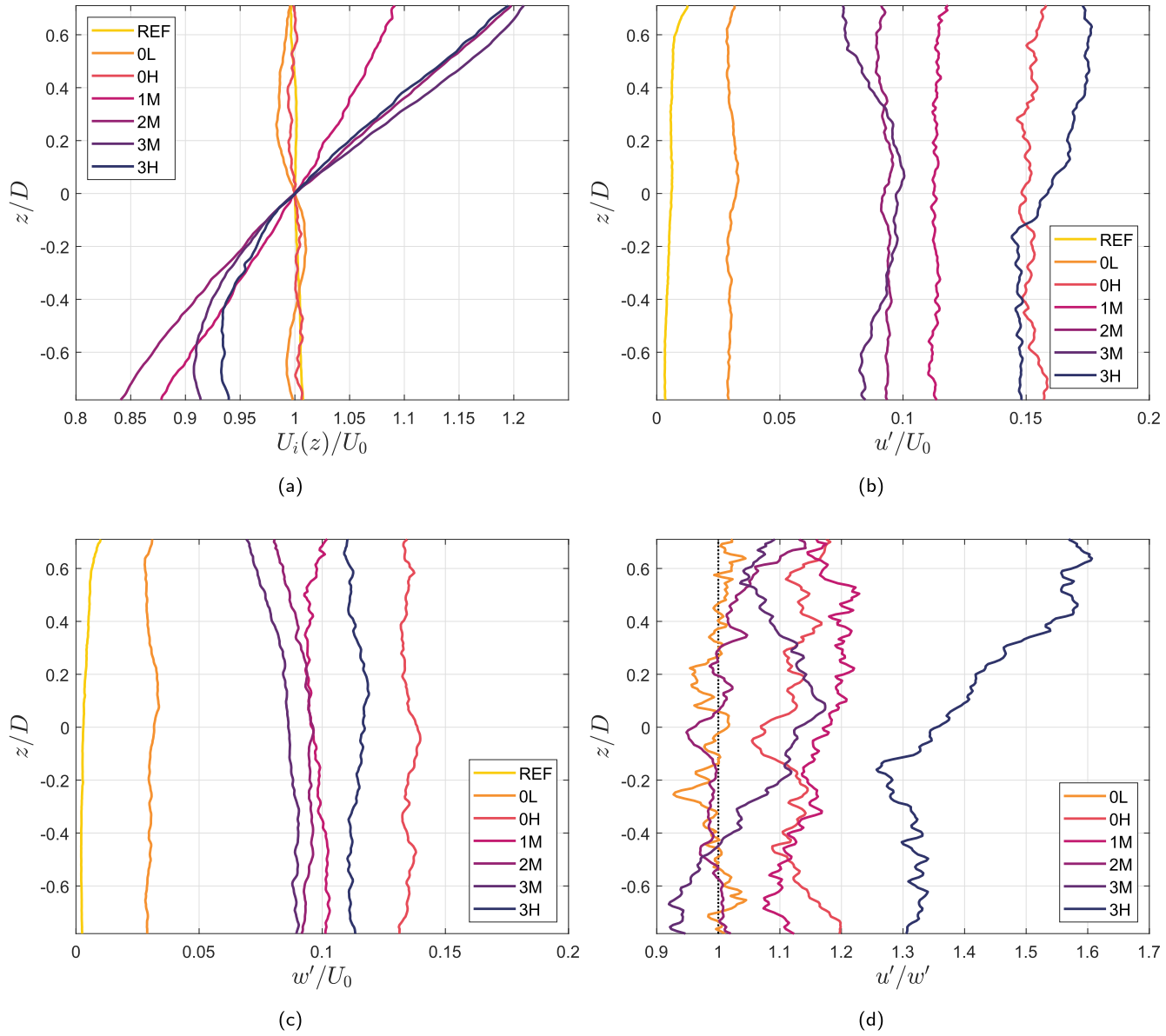

Fig. 4. Flow profiles of a) normalized mean streamwise velocity U_i/U_0, b) u'$/U_0$, and c) w'$/U_0$ for all cases; d) u'/w' for all cases with active grid installed. z-axis is normalized by rotor diameter $D = 0.21$ m.

Table 1
Summary of incoming flow characteristics at $x/D = -0.7$.

Mode	α	u'$_0/U_0$ [%]	U_{eq}/U_0	$U_{eq,turb}/U_0$
REF	0	0.6	1.000	1.000
0L	0	3.2	0.997	0.998
0H	0	14.8	0.999	1.021
1M	0.17	11.2	1.001	1.013
2M	0.29	9.2	1.008	1.017
3M	0.29	9.7	1.015	1.024
3H	0.24	15.8	1.012	1.036

shown in Fig. 8a. The wake boundary is calculated by subtracting the freestream mean velocity profile from the overall velocity field and tracing $(U - U_i)/U_0 = 0$. The wake centre is defined as the local minimum in the $(U - U_i)/U_0$ field in the region along the hub centre. It can be seen that the wake boundaries for all cases stay relatively symmetrical about the hub, with no indication of deflection. The different incoming shear profiles and turbulence intensities appear to have no significant impact on the behaviour of the wake boundaries within the investigated region, when the wake is defined relative to the incoming flow. The same is true of the wake centrelines.

The hub velocity contour line is defined as the trace where $(U - U_0)/U_0 = 0$, or where the velocity in the field is equal to the hub centreline velocity U_0. Fig. 8b shows the contour lines for all the test cases. For uniform flow conditions, these contour lines coincide with the wake boundary and originate from the rotor blade tips. In sheared flows, they are deflected toward the high-velocity side of the incoming shear flow and continue in the wake. Compared to the uniform flow cases, shear flows force the hub velocity contour lines from the blade tip toward the hub, and this forcing increases with local shear gradient. This phenomenon may result from the higher momentum carried by the high-velocity flow in the cases with more shear overcoming the radial flow induced by the rotor. The z/D location of the contour lines in the near-field wake can also be

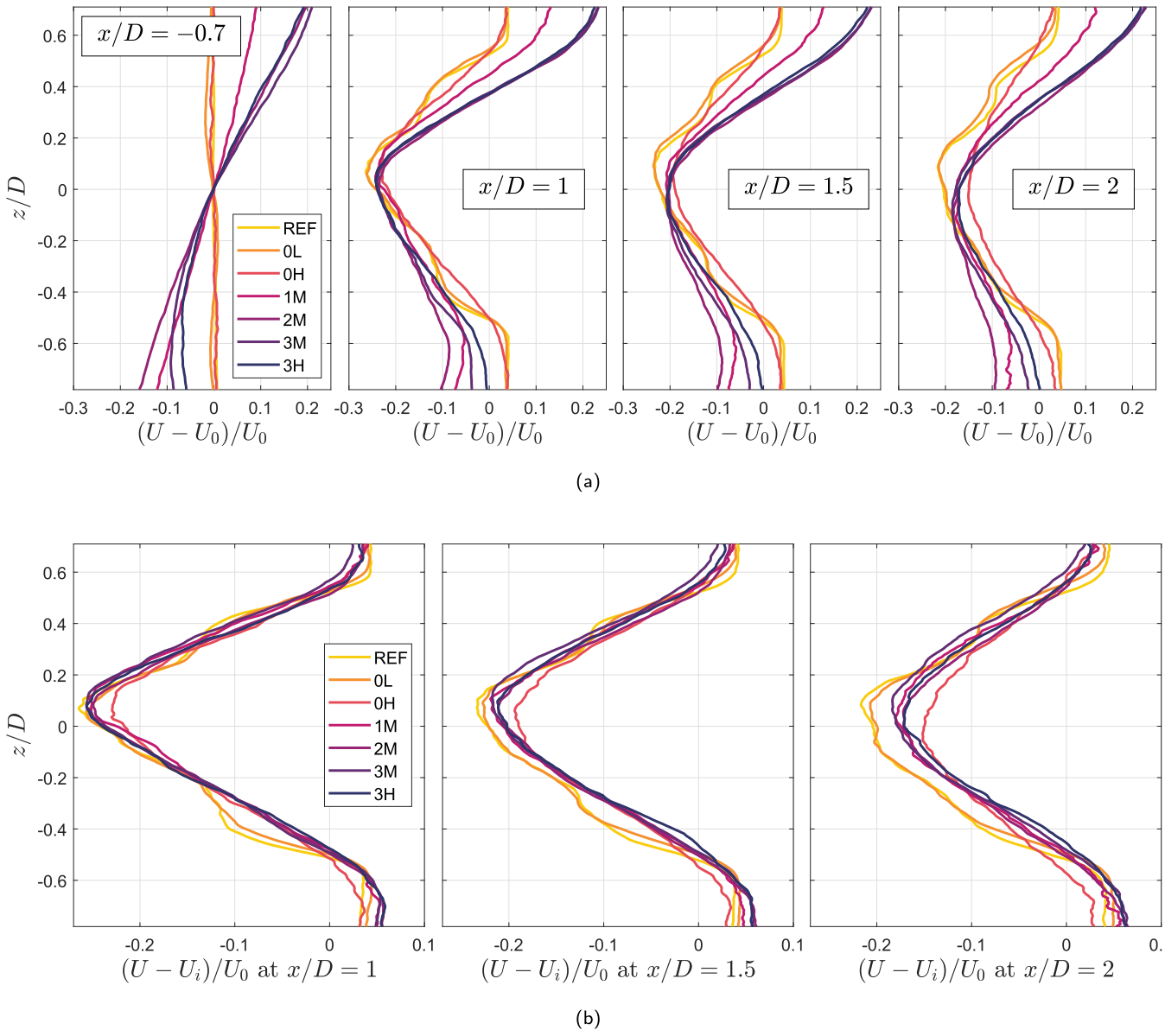

Fig. 5. Two representations of wake profiles at $x/D = 1, 1.5, \& 2$ for all cases, where a) is normalized with respect to hub centreline velocity, and b) has their respective freestream velocity profiles removed and normalized by hub centreline velocity. Incoming mean velocity profile is also shown in a), centred at $x/D = -0.7$.

used as a measure of the severity of shear in the absolute wake velocity profile on the high-velocity side. As U_0 is similar for all test cases ($\sim 10 \text{ms}^{-1}$) and it is shown in Fig. 5a that all cases have similar minimum velocity deficit in the wake, the contour lines mark the z/D location where the velocity field must return to U_0. Thus, the closer the contour lines are to the hub, the greater the velocity gradient in the wake must be.

5. Turbulence statistics

In Fig. 5a, it can be seen that the absolute wake velocity gradient on the high-velocity side in a shear flow is higher than the uniform flow cases, while the opposite is true on the low-velocity side. This difference in the shear gradient has an impact on the turbulence statistics distributions in the near-field wake. Fig. 9 shows the u', w', and turbulence isotropy (u'/w') profiles in the wake normalized by the hub centreline velocity U_0, at streamwise locations $x/D = 1$, 1.5, & 2. Case 1M at $x/D = 2$ is not shown in these profiles because of data noise contamination for $z/D \lesssim -0.4$, which increased the calculated values for u' and w', and therefore is not representative of the actual distribution profile. The u' fluctuations for the uniform flow cases show two peaks in its spanwise wake distribution, one at each of the blade tips. The prominence of these peaks decreases downstream. This is expected as vortex streaks trailing the blade tips lead to higher production of turbulence [32]. The turbulence intensity reached in the wake for case 0H is comparable to that of the incoming flow. In the shear flow cases, velocity fluctuations are not evenly distributed in the spanwise direction. Instead they are biased toward the high-velocity side of the shear flow. This behaviour is consistent with the observation of Chamorro & Porté-Agel [32]. This observation suggests that higher shear leads to higher velocity fluctuations, or turbulence intensity, in the wake.

The w' fluctuations for cases REF and 0L show 4 distinct peaks at $x/D = 1$, associated with vortex shedding from the blade tips and root. Case 0H at the same location does not show these 4 peaks in w' distribution, suggesting that the higher freestream turbulence

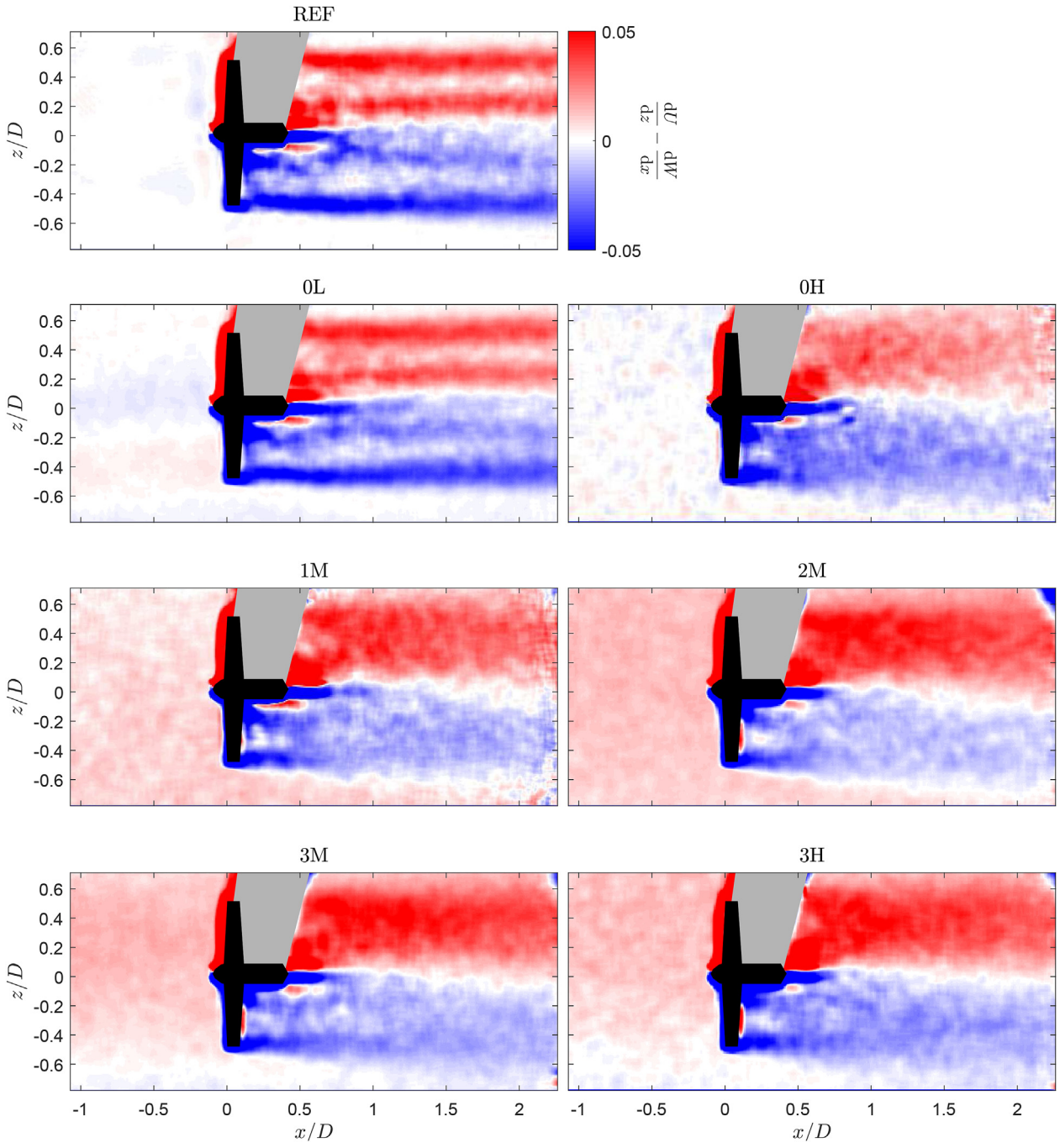

Fig. 6. Averaged vorticity fields for all 7 test cases.

level was sufficient to mix w' into a more uniform distribution. The two peaks associated with the root decay faster than those associated with the tip as the flow progresses downstream in the wake, and they largely disappear by $x/D = 2$, leaving only the two blade tip peaks present in the w' distribution. For the shear flow cases, w' distribution, similar to u', is biased toward the high-velocity side.

Fig. 9c shows the u'/w' profiles in the wake. For cases REF and 0L, there are two prominent peaks associated with the blade tips where $u'/w' > 1$. The flow is more isotropic near the hub ($u'/w' \approx 1$). These two peaks decrease in size downstream, and at $x/D = 2$ are no longer noticeable, and the whole wake region becomes isotropic. This phenomenon is only observed for cases REF and 0L, not 0H, suggesting that increased incoming turbulence level impacts the wake's turbulence isotropy. For case 0H, the wake turbulence is only near isotropic within a narrow region centred about the hub, and anisotropy increases to about the incoming flow level toward the blade tips. At $x/D = 2$, the flow is no longer near isotropic even at the hub centreline. Another interesting phenomenon for cases REF and 0L is that $u'/w' < 1$ just outside of the turbine radius. This only appears for these two cases, and could be due to the blade tip induced radial velocity component promoting w' fluctuation as it "sheds" from the rotor, and increased incoming turbulence level suppresses this action. For the shear flows, the wake turbulence isotropy is asymmetric. The flow is near isotropic

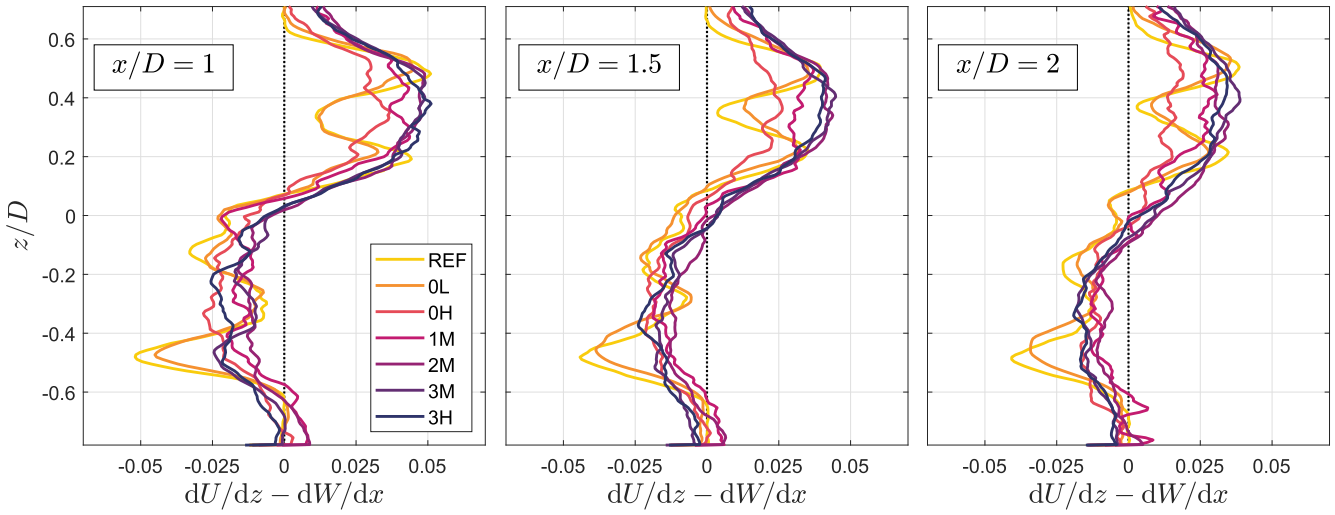

Fig. 7. Vorticity wake profiles at $x/D = 1, 1.5, \& 2$ for all cases.

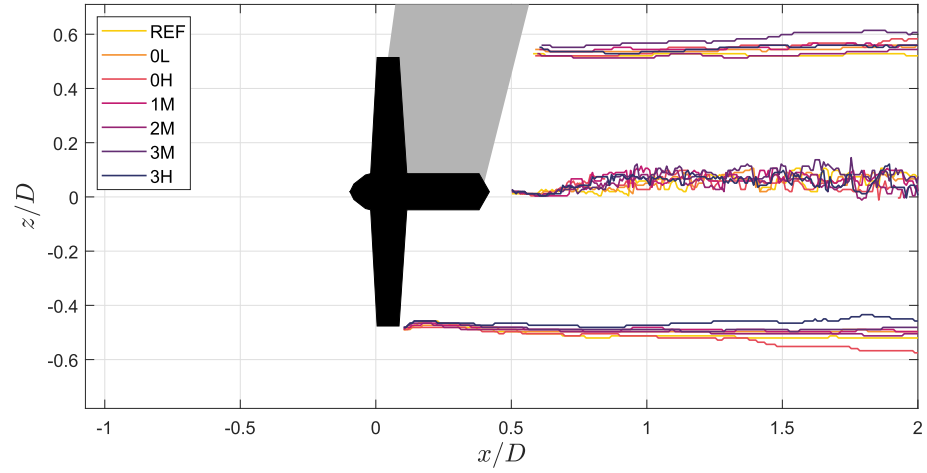

(a)

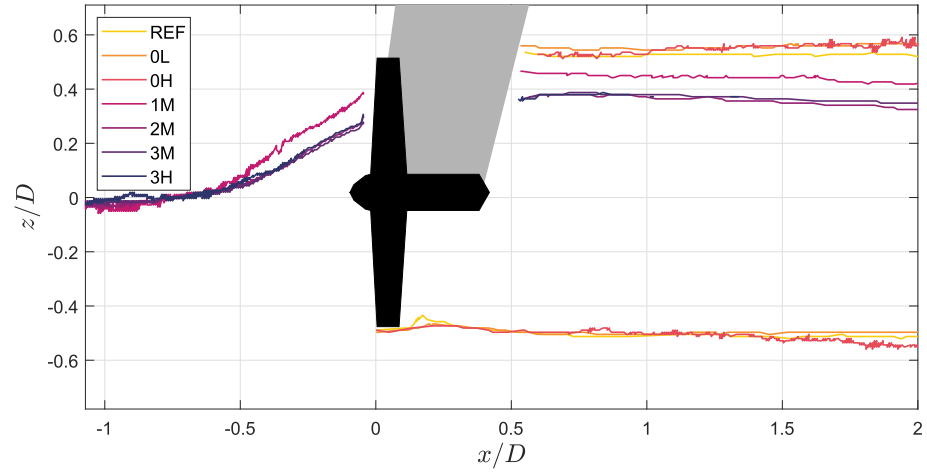

(b)

Fig. 8. a) Wake centreline and boundary of all test cases. b) Hub centreline velocity contour for all test cases.

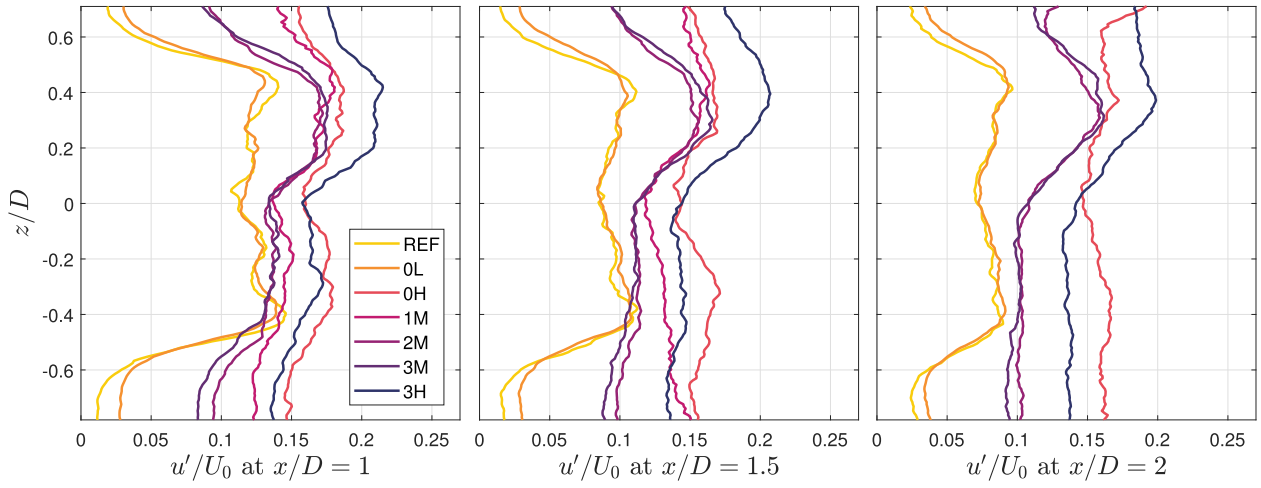

(a)

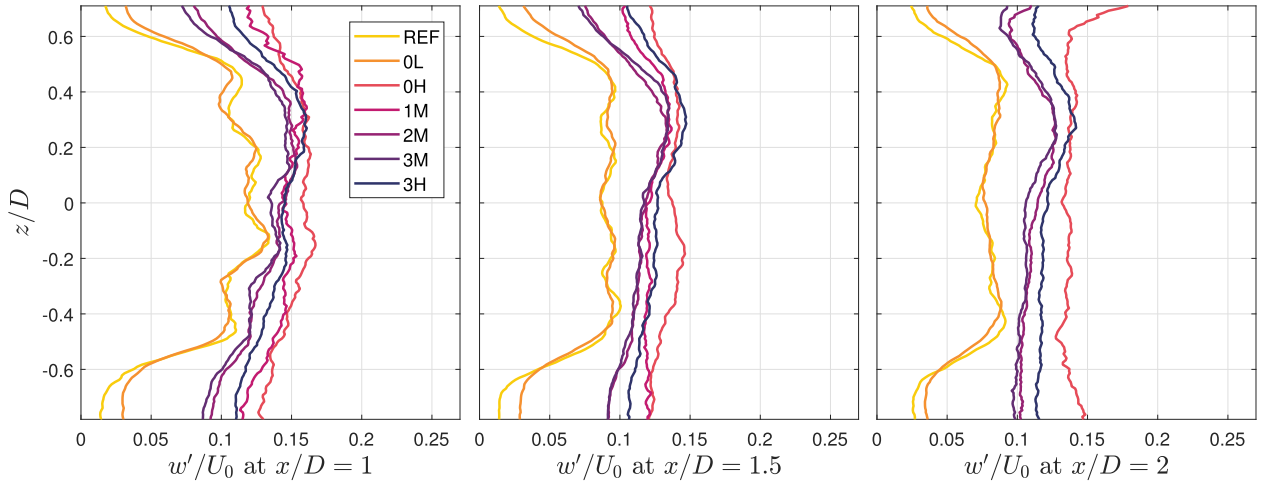

(b)

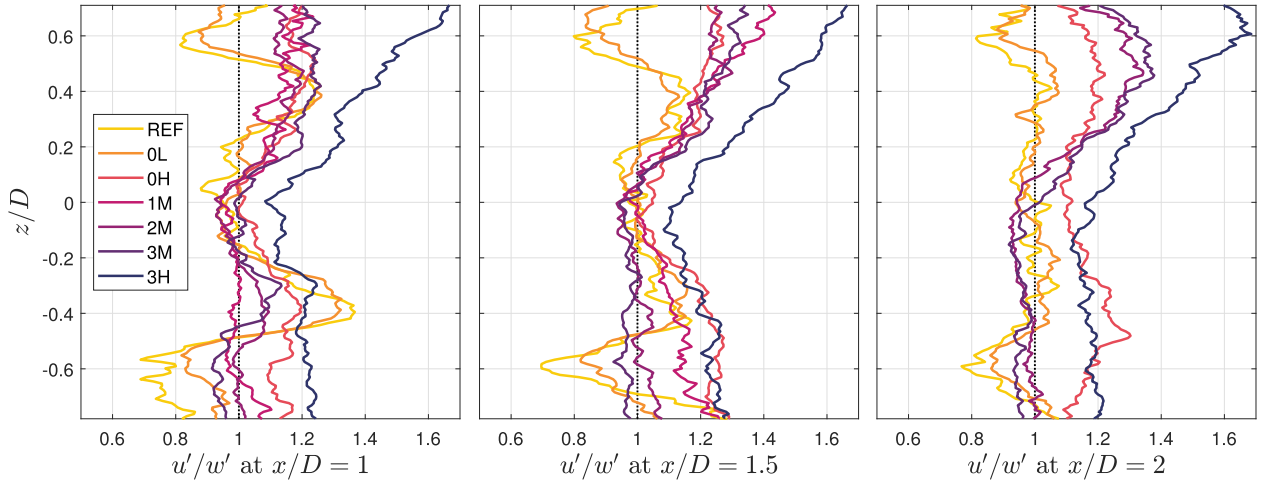

(c)

Fig. 9. a) u'/U wake profiles, b) w'/U wake profiles, and c) turbulence isotropy (u'/w') at x/D = 1, 1.5, & 2 for all cases.

on the low-velocity half of the flow, and more anisotropic on the high-velocity side. This suggests that on top of promoting velocity fluctuations, high shear in the wake also promotes streamwise fluctuations over spanwise. Overall, it appears that both u'_0/U_0 and the shear profile affect the near-wake isotropy, with u'_0/U_0 having more local effects near the hub and blade tips, and the shear profile having a global effect on the symmetry of the isotropy distribution.

The bias of velocity fluctuation toward the high-velocity side in shear flow cases can be seen more prominently in the Reynolds shear stress $-\overline{u'w'}$ distribution shown in Fig. 10. In the uniform flow cases REF, 0L, and 0H, the Reynolds shear stress is symmetric about the hub centreline, with a positive peak located roughly at $z/D = 0.25$, half the distance between the blade tip and the hub centre, and a negative peak at $z/D = -0.25$. The magnitude of the peaks in Reynolds shear stress increases with increasing u'/U. For shear flow cases, the magnitude for the positive peaks on the high-velocity side is significantly higher than that of the negative peaks on the low-velocity side, akin to the asymmetry in the velocity fluctuations. Increasing u'_0/U_0 also increases the local peak magnitudes in Reynolds shear stress distribution for shear flows. The difference diminishes as the flow moves downstream. The different shear levels do not appear to significantly impact the shape of the distribution aside from asymmetry, suggesting that u'_0/U_0 has a greater impact on the Reynolds shear stress for both uniform and shear flows. However, the shear enhances the positive peak while suppressing the negative peak. The degree of reduction in the negative peak resulting from the shear is greater than the degree of enhancement of the positive peak. The Reynolds shear stress has a significant impact on the cross-terms in the production of the total turbulent kinetic energy budget. The combined effects of large values of $-\overline{u'w'}$ and $\partial U/\partial z$ in the high-velocity region in the near wake is expected to have a large influence on the distribution of the turbulent kinetic energy production.

The production $\Sigma u'_i u'_j \frac{dU_i}{dx_j}$ was examined term-by-term to determine the contribution of each component. The term $-\overline{u'w'}\frac{\partial W}{\partial x}$ was found to be negligible compared to the other three terms, and therefore was not included in the sum. This is due to the relatively small variations in W with respect to x in the wake. Note that we only have four components in total because these are 2D flow data. Fig. 11 reveals that there is a higher peak in turbulence production on the high-velocity side for shear flow cases. In particular, case 1M shows a double-peak structure at $x/D = 1.5$ on the high-velocity side, while the other shear cases all show a single peak. At $x/D = 2$, the double-peak in 1M have blended into one. The presence and later mixing of the two peaks suggests an increase in turbulence production in the streamwise direction for case 1M, whereas the presence of a single peak throughout the wake for the other shear flow cases suggests that turbulence production was already high enough to promote mixing into one region, which is consistent with the findings of Rockel et al. [23]. This observation suggests that turbulence production distribution is affected more by shear profile than u'/U in the near-field wake, as case 1M differs most significantly from the other shear cases in local velocity gradient. Turbulence intensity, however, does have an impact on the level of turbulence production, as case 3H shows higher level than cases 2M and 3M.

Fig. 7 shows the vorticity distribution in the wake. As mentioned in the previous section, the REF and 0L cases have a double-peak structure on either side of the hub, associated with vortex streams from the blade tip and the hub. In case 0H these two peaks are blended into one, centred around the middle of the blades. In the shear flow cases, the magnitude of vorticity peak on the high-velocity side is again greater than that on the low-velocity side, consistent with the other observation of biased turbulence production. This would also suggest that vorticity in the near-field wake is more significantly affected by shear than freestream turbulence intensity. It is interesting to note that u'/U has no significant impact on vorticity level. In Fig. 6, aside from showing vortex stream blending due to increased u'/U, it also shows the promotion of vorticity magnitude on the high-velocity side.

The formulations of the equivalent velocity U_{eq} of Wagner et al. [7] (Eq. (2)) and $U_{eq,turb}$ of Choukulkar et al. [11] (Eq. (3)) differ in that Choukulkar et al. [11] consider the effects of u'_0/U_0 and wind angle. Adapting the U_{eq} formulations of both authors to the near wake region can give another measure of how shear profiles and turbulence intensity levels impact the available kinetic energy for the downstream turbine. Fig. 12 shows the percentage difference between U_{eq} and $U_{eq,turb}$ for all the cases. Choukulkar et al. [11]'s formulation is consistently higher than that of Wagner et al. [7] because velocity fluctuations are considered. It thus appears that u'_0/U_0 has a greater impact on the available energy than the shear profile as the data points are roughly separated into three groups of differing u'_0/U_0, regardless of the shear profile. The two cases with the highest u'_0/U_0, 0H and 3H, show an increase in the equivalent wind speed by $\sim 4\%$ at $x/D = 1$, and by $\sim 3\%$ at $x/D = 2$.

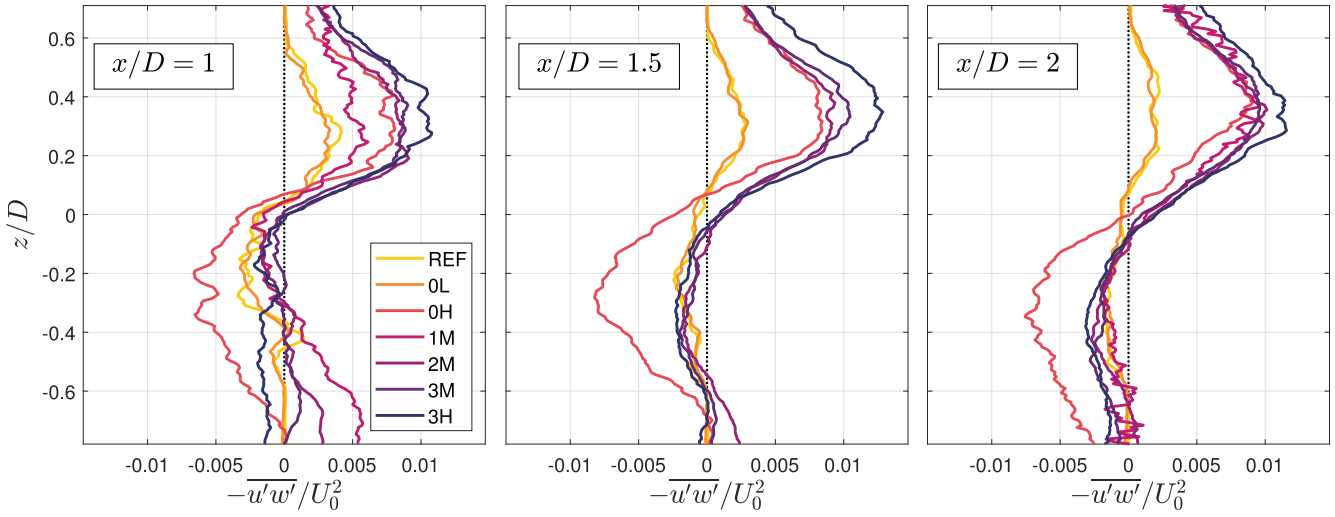

Fig. 10. Non-dimensional Reynolds shear stress wake profiles at $x/D = 1$, 1.5, & 2 for all cases.

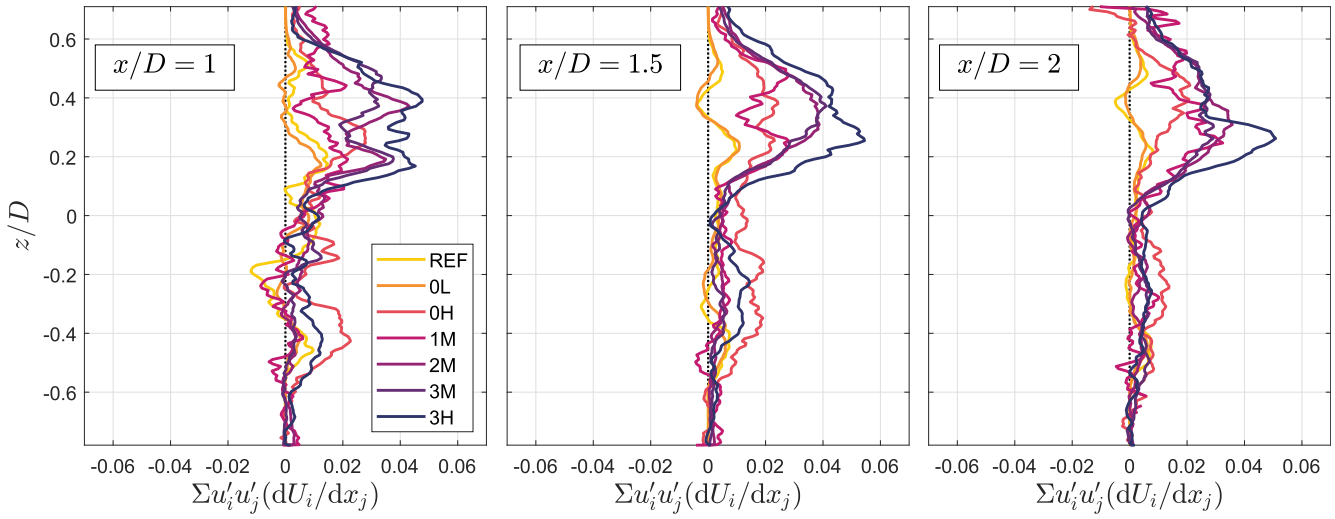

Fig. 11. Turbulence production wake profiles at $x/D = 1$, 1.5, & 2 for all cases.

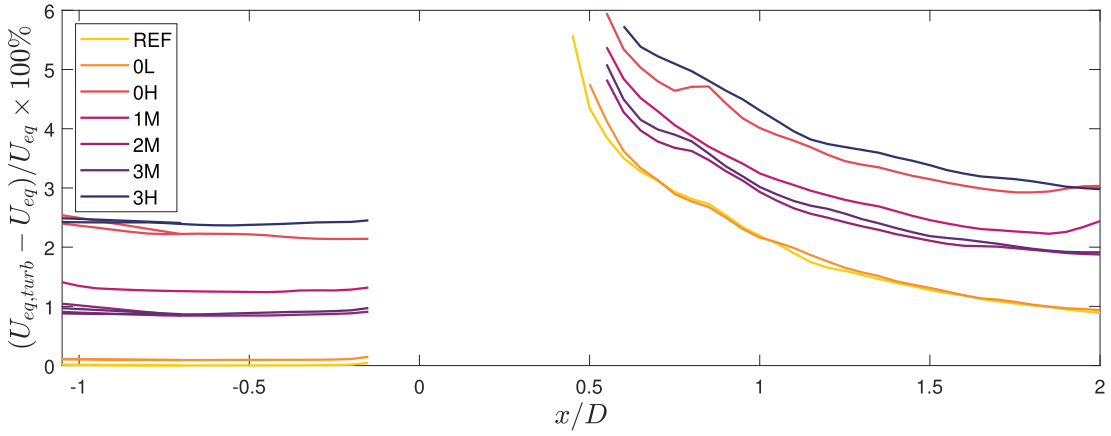

Fig. 12. Percentage differences between U_{eq} and $U_{eq,turb}$ [7].'s formulation is used for U_{eq} and [11]'s formulation is used for $U_{eq,turb}$; differences are shown for upstream and downstream of the turbine for all cases.

The above observation is interesting when it is compared to the torque, and thus power, measurements performed here. In general, the difference in mean power (P) between all cases investigated does not exceed the uncertainty of the sensor. Despite the increased 'relative' energy between the two estimates for the equivalent wind speed presented in Fig. 12, their actual values (reported in Table 1) do not vary significantly between test cases. For instance, the peak-to-peak variation between all test cases is 1.8% for U_{eq} and 3.8% for $U_{eq,turb}$, respectively, where the latter considers the effect of the turbulence intensity in addition to the shear. Given such a small change to the equivalent wind speed, it is perhaps not surprising that the mean power did not change significantly. One must also consider that the shears investigated here are significant, some on the order of 30% change in U across the rotor diameter. The fact that this does not significantly change the equivalent wind estimates or the mean power for a fixed U_0 suggests that it is the absolute value of the hub velocity rather than the meticulous integration of shear that dominates the strong collapse presented in, for instance, Wagner et al. [6], over the entire wind turbine operational range. What is interesting in the present results though is that the standard deviation of the power (p') calculated for frequencies below the rotational rate of the turbine appears to have a linear dependence on the incoming turbulence intensity as illustrated in Fig. 13. Thus, while there are no obvious mean changes to the power extraction, the turbulence intensity certainly impacts the power

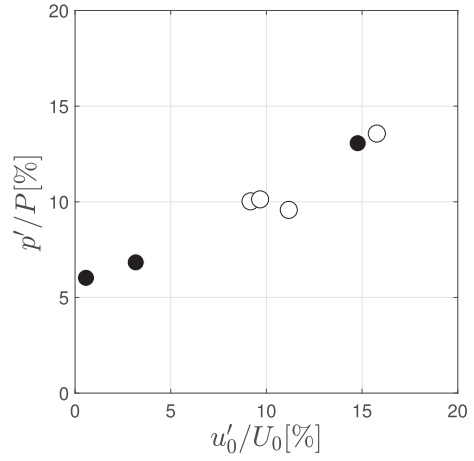

Fig. 13. Variation of power fluctuations measured on the turbine rotor compared to the incoming flow turbulence intensity. Filled symbols are in uniform incoming flows, and empty symbols are the sheared cases.

fluctuations, which would in turn have implications for the turbine lifetime.

It is of note that at $u'/U = 3.2\%$, case 0L has near-identical distributions of all the wake turbulence statistics analyzed as the reference case, suggesting that this level of turbulence intensity is not sufficient to significantly impact the turbulence properties in the wake. The only place it appears to have had an impact is to increase the fluctuations in the power output of the rotor.

6. Conclusions

This study investigated the independent effects of incoming shear and turbulence intensity on the near-field wake of a lab-scale wind turbine. A total of seven different flow fields were generated using an active grid. This approach allowed for a larger range of incoming flow conditions to be assessed than previously achievable with conventional means. The mean velocity field in the wake was examined, and it was found that the absolute velocity deficit can be linearly decomposed into a symmetric relative velocity deficit and the incoming shear profile. This shows that the mean velocity field of the near-wake region of a wind turbine is relatively robust to different types of incoming flow, and highlights a universality of the turbine wake when the incoming flow is removed. This has the implication that the mean wake can be estimated based on uniform flow, and a non-uniform incoming condition can be simply superimposed later. A similar idea was proposed by Chamorro & Porté-Agel [32], but has been assessed and confirmed in a wider range of incoming flow conditions here.

The hub velocity contour line was found to be biased toward the high velocity side of a shear flow. Increasing the shear forced this contour line toward the hub and away from the blade tips. This was attributed to higher momentum in the high-velocity flow overcoming the local outward radial flow induced by the spinning rotor. Examination of the turbulence statistics showed that both turbulence production and vorticity were biased toward the high-velocity side in the shear flows as well. In particular, the spatial distribution of the production and vorticity were highly dependent on the profile of the incoming flow, while the incoming turbulence intensity dominated the magnitude of the production. These phenomena in turn led to higher velocity fluctuations on the high-velocity side of sheared cases. Interestingly, the surrogate power measurements of the present study illustrated that the mean power did not change substantially for the various test cases investigated. However, the power fluctuations appear to have an approximately linear dependence on the incoming turbulence intensity, regardless of the degree of shear. This has repercussions for the lifetime of turbine, suggestion that increased turbulence will reduce total lifetime. It should also be noted that for a uniform flow with incoming turbulence intensity less than 3.2%, the wake properties are nearly-identical to those from the reference quasi-laminar incoming flow.

The experimental setup of this study permitted investigations of the wake up to $x/D = 2$. Future studies should investigate the medium- to far-field of the wake in order to better understand its development and the consequent impact on turbines located downstream. In particular, measurements farther downstream could allow for the development of a new wake model that incorporates the effects of shear and turbulence intensity presented herein. It should also be noted that in a real-world scenario, the rotor wake also interacts with the wake from the tower, causing the centre of the vortex core to be deflected downward towards the ground, leading to asymmetry in the wake geometry [34]; this phenomenon is absent from the present study as a result of the low drag sting used to hold the turbine in the centre of the flow, and would be an interesting topic for future investigations. Finally, this study has been presented as a proof-of-concept for the approach of placing a model wind turbine downstream of an active grid that can produce a wide range of turbulent shear flows. It was demonstrated that the shear and turbulence intensity of the incoming conditions could be changed in a controllable way, and that these changes had an impact on the power and wake of the model turbine. Future studies should apply similar methodology to larger scale models that can more closely match the operating conditions and geometries of full-scale wind turbines. Such facilities already exist in several larger scale labs around the world.

Declaration of competing interest

The authors declare that they have no known competing financial interests or personal relationships that could have appeared to influence the work reported in this paper.

Acknowledgements

The authors gratefully acknowledge the financial support of the EPSRC and NSERC.

The authors declare that they have no conflicts of interest that impact this study.

BG and RJH conceived of the idea for this work. MAF designed the model turbine. RJH conducted the experiments with help from MAF. LL performed the analysis and was the primary author of the manuscript with support from RJH. All authors read and contributed to the manuscript.

Preliminary results from this work were presented at the *Interdisciplinary Turbulence Initiative Conference* in Bertinoro, Italy in 2018 [35]. The present investigation covers significantly more breadth and is wholly original.

References

[1] M.S. Adaramola, P. Krogstad, Experimental investigation of wake effects on wind turbine performance, Renew. Energy 36 (2011) 2078–2086, https://doi.org/10.1016/j.renene.2011.01.024.

[2] R.J. Barthelmie, S.C. Pryor, S.T. Frandsen, K.S. Hansen, J.G. Schepers, K. Rados, W. Schlez, A. Neubert, L.E. Jensen, S. Neckelmann, Quantifying the impact of wind turbine wakes on power output at offshore wind farms, J. Atmos. Ocean. Technol. 27 (2010), https://doi.org/10.1175/2010JTECHA1398.1.

[3] M. Gaumond, P.E. Réthoré, A. Bechmann, S. Ott, G.C. Larsen, A. Peña, K.S. Hansen, Benchmarking of wind turbine wake models in large offshore wind farms, in: Proceedings of the Science of Making Torque from Wind 2012, 2012.

[4] L.J. Vermeer, J.N. Sørensen, A. Crespo, Wind turbine wake aerodynamics, Prog. Aerosp. Sci. 39 (2003) 467–510, https://doi.org/10.1016/S0376-0421(03)00078-2.

[5] F.D. Bianchi, H. de Battista, R.J. Mantz, Wind Turbine Control Systems: Principles, Modelling, and Gain Scheduling Design, Springer, 2006.

[6] R. Wagner, M. Courtney, J. Gottschall, P. Lindelöw-Marsden, Accounting for the speed shear in wind turbine power performance measurement, Wind Energy 14 (2011) 993–1004, https://doi.org/10.1002/we.509.

[7] R. Wagner, I. Antoniou, S.M. Pedersen, M.S. Courtney, H.E. Jørgensen, The influence of the wind speed profile on wind turbine performance measurements, Wind Energy 12 (2009) 348–362, https://doi.org/10.1002/we.297.

[8] N. Dimitrov, A. Natarajan, M. Kelly, Model of wind shear conditional on turbulence and its impact on wind turbine loads, Wind Energy 18 (2015) 1917–1931, https://doi.org/10.1002/we.1797.

[9] T. Mücke, D. Kleinhans, J. Peinke, Atmospheric turbulence and its influence on the alternating loads on wind turbines, Wind Energy 14 (2011) 301–316, https://doi.org/10.1002/we.422.

[10] P. Milan, M. Wächter, J. Peinke, Turbulent character of wind energy, Phys. Rev. Lett. 110 (2013), https://doi.org/10.1103/PhysRevLett.110.138701.

[11] A. Choukulkar, Y. Pichugina, C. Clark, R. Calhoun, R. Banta, A. Brewer, M. Hardesty, A new formulation for rotor equivalent wind speed for wind resource assessment and wind power forecasting, Wind Energy 19 (2016) 1439–1452, https://doi.org/10.1002/we.1929.

[12] J. Counihan, An improved method of simulating an atmospheric boundary layer in a wind tunnel, Atmos. Environ. 3 (1969) 197–214, https://doi.org/10.1016/0004-6981(69)90008-0.

[13] J. Counihan, Simulation of an adiabatic urban boundary layer in a wind tunnel, Atmos. Environ. 7 (1973) 673–689, https://doi.org/10.1016/0004-6981(73)

90150-9.
[14] C. Vanderwel, S. Tavoularis, Coherent structures in uniformly sheared turbulent flow, J. Fluid Mech. 689 (2011) 434–464, https://doi.org/10.1017/jfm.2011.423.
[15] D. Medici, P.H. Alfredsson, Measurements on a wind turbine wake: 3D effects and bluff body vortex shedding, Wind Energy 9 (2006) 219–236, https://doi.org/10.1002/we.156.
[16] Y. Hattori, M. Yamamoto, Y. Eguchi, K. Kondo, H. Suto, N. Tanaka, A Wind Tunnel Experiment on Wake Structure of a Wind Turbine, KAJIM Technical Research Institute, Kajim, 2007, https://doi.org/10.13140/2.1.5141.0727.
[17] H. Makita, Realization of a large-scale turbulence field in a small wind tunnel, Fluid Dyn. Res. 8 (1991) 53–64, https://doi.org/10.1016/0169-5983(91)90030-m.
[18] P. Knebel, A. Kittel, J. Peinke, Atmospheric wind field conditions generated by active grids, Exp. Fluid 51 (2011) 471–481, https://doi.org/10.1007/s00348-011-1056-8.
[19] I. Neunaber, J. Schottler, J. Peinke, M. Hölling, Comparison of the development of a wind turbine wake under different inflow conditions, in: R. Örlü, A. Talamelli, M. Oberlack, J. Peinke (Eds.), Progress in Turbulence VII, Springer International Publishing, Cham, 2017, pp. 177–182, https://doi.org/10.1007/978-3-319-57934-4_25.
[20] X. Shen, Z. Warhaft, The anisotropy of the small scale structure in high Reynolds (R_λ~1000) turbulent shear flow, Phys. Fluids 12 (2000), https://doi.org/10.1063/1.1313552.
[21] H.E. Cekli, W. van de Water, Tailoring turbulence with an active grid, Exp. Fluid 49 (2010) 409–416, https://doi.org/10.1007/s00348-009-0812-5.
[22] J. Schottler, A. Hölling, J. Peinke, M. Hölling, Brief communication: on the influence of vertical wind shear on the combined power output of two model wind turbines in yaw, Wind Energy Sci. 2 (2017) 439–442, https://doi.org/10.5194/wes-2-439-2017.
[23] S. Rockel, J. Peinke, M. Hölling, R.B. Cal, Dynamic wake development of a floating wind turbine in free pitch motion subjected to turbulent inflow generated with an active grid, Renew. Energy 112 (2017) 1–16, https://doi.org/10.1016/j.renene.2017.05.016.
[24] M. Talavera, F. Shu, Experimental study of turbulence intensity influence on wind turbine performance and wake recovery in a low-speed wind tunnel, Renew. Energy 109 (2017) 363–371, https://doi.org/10.1016/j.renene.2017.03.034.
[25] R.J. Hearst, B. Ganapathisubramani, Tailoring incoming shear and turbulence profiles for lab-scale wind turbines, Wind Energy 20 (2017) 2021–2035, https://doi.org/10.1002/we.2138.
[26] E. Dogan, R. Hanson, B. Ganapathisubramani, Interactions of large-scale free-stream turbulence with turbulent boundary layers, J. Fluid Mech. 802 (2016) 79–107, https://doi.org/10.1017/jfm.2016.435.
[27] R.J. Hearst, P. Lavoie, The effect of active grid initial conditions on high Reynolds number turbulence, Exp. Fluid 56 (2015) 1–20, https://doi.org/10.1007/s00348-015-2052-1.
[28] J. Jonkman, S. Butterfield, W. Musial, G. Scott, Definition of a 5-MW Reference Wind Turbine for Offshore System Development, Technical Report, National Renewable Energy Laboratory, 2009, https://www.nrel.gov/docs/fy09osti/38060.pdf.
[29] D.B. Araya, J.O. Dabiri, A comparison of wake measurements in motor-driven and flow-driven turbine experiments, Exp. Fluid 56 (2015), https://doi.org/10.1007/s00348-015-2022-7.
[30] F.D. Bianchi, R.J. Mantz, H.D. Battista, The Wind and Wind Turbines, Springer, 2007.
[31] S. Corrsin, Turbulence: experimental methods, in: S. Flügge, C. Truesdell (Eds.), Handbuch der Physik, Springer, 1963, pp. 524–589.
[32] L.P. Chamorro, F. Porté-Agel, A wind-tunnel investigation of wind-turbine wakes: boundary-layer turbulence effects. Bound, Layer Meteor. 132 (2009) 129–149, https://doi.org/10.1007/s10546-009-9380-8.
[33] Y. Jin, H. Liu, R. Aggarwal, A. Singh, L.P. Chamorro, Effects of freestream turbulence in a model wind turbine wake, Energies 9 (2016), https://doi.org/10.3390/en9100830.
[34] F. Pierella, L. Sætran, Wind tunnel investigation on the effect of the turbine tower on wind turbines wake symmetry, Wind Energy 20 (2017) 1753–1769, https://doi.org/10.1002/we.2120.
[35] L. Li, R. Hearst, B. Ganapathisubramani, The mean velocity of the near-field of a lab-scale wind turbine in tailored turbulent shear flows, in: R. Örlu, A. Talamelli, M. Oberlack, J. Peinke (Eds.), Progress in Turbulence VIII, Springer Proceedings in Physics, 2019, pp. 317–322, https://doi.org/10.1007/978-3-030-22196-6_50.